Nanoparticulate fillers improve the mechanical strength of bone cement

Andreas H Gomoll, Wolfgang Fitz, Richard D Scott, Thomas S Thornhill, and Anuj Bellare

Department of Orthopaedic Surgery, Brigham and Women's Hospital, Harvard Medical School, Boston, MA, USA
Correspondence AHG: agomoll@yahoo.com
Submitted 07-07-28. Accepted 07-12-02

Background and purpose **Polymethylmethacrylate-(PMMA-) based bone cement contains micrometer-size barium sulfate or zirconium oxide particles to radiopacify the cement for radiographic monitoring during follow-up. Considerable effort has been expended to improve the mechanical qualities of cements, largely through substitution of PMMA with new chemical structures. The introduction of these materials into clinical practice has been complicated by concerns over the unknown long-term risk profile of these new structures in vivo. We investigated a new composite with the well-characterized chemical composition of current cements, but with nanoparticles instead of the conventional, micrometer-size barium sulfate radiopacifier.**

Methods **In this study, we replaced the barium sulfate microparticles that are usually present in commercial PMMA cements with barium sulfate nanoparticles. The resultant "microcomposite" and "nanocomposite" cements were then characterized through morphological investigations such as ultra-small angle X-ray scattering (USAXS) and scanning electron microscopy (SEM). Mechanical characterization included compression, tensile, compact tension, and fatigue testing.**

Results **SEM and USAXS showed excellent dispersion of nanoparticles. Substitution of nanoparticles for microparticles resulted in a 41% increase in tensile strain-to-failure ($p = 0.002$) and a 70% increase in tensile work-of-fracture ($p = 0.005$). The nanocomposite cement also showed a two-fold increase in fatigue life compared to the conventional, microcomposite cement.**

Interpretation **In summary, nanoparticulate substitution of radiopacifiers substantially improved the in vitro mechanical properties of PMMA bone cement without changing the known chemical composition.**

Commercial acrylic or polymethylmethacrylate (PMMA) bone cements have been used successfully in total joint replacement surgery for over four decades, and have been thoroughly characterized (Saha and Pal 1984, Krause and Mathis 1988, Demian and McDermott 1998, Lewis 2003). Fatigue and fracture properties of cement continue to be investigated since cement failure can lead to undesirable particle shedding or fracture. PMMA cements contain approximately 10 per cent by weight of a radiopacifier, most commonly barium sulfate or zirconium oxide particles measuring 1–3 μm in diameter. The high viscosity of cements during mixing complicates even particle dispersion throughout the polymer matrix, resulting in the presence of large domains with agglomerated filler particles.

Poor dispersion of radiopacifiers or other additives can affect both crack initiation and crack propagation in the hardened cement (Topoleski et al. 1990). Fatigue cracks mainly propagate within the inter-bead matrix regions that contain the radiopacifiers (Topoleski et al. 1993). In the latter study, it was also observed that radiopacifier aggregates were not bonded to the PMMA surrounding them. Thus, from the standpoint of defect concentration in bone cement, radiopacifier agglomerates act as sites of high stress concentration and consequently weaken the cement.

In this study, we substituted the micrometer-size barium sulfate radiopacifier particles with an identical amount of 100-nm-size barium sulfate particles in commercial bone cement. We hypothesized that if uniformly dispersed in the cement, smaller radiopacifier nanoparticles would lead to smaller

DOI 10.1080/17453670710015349

Table 1. Mechanical tests and respective specimens fabricated from bone cement

Test	Specimen type
Compression	Cylindrical specimen, ASTM F451-99
Tensile	Type V dumb-bell specimen, ASTM D638-97
Compact tension	Prenotched pin-loaded specimen
Fatigue	Prenotched dog-bone specimen
Electron microscopy (SEM)	Freeze-fractured specimens
X-ray scattering (USAXS)	Sheet, 0.5 mm in thickness

pores surrounding the non-bonded barium sulfate particles in the inter-bead matrix region of the cement, thereby reducing defect size and improving mechanical properties.

Methods

Cement and specimen preparation

We used CMW1 bone cement (DePuy Orthopaedics Inc., Warsaw, IN) in all experiments, since the powder component of this cement does not contain premixed barium sulfate. The basic CMW1 powder served as radiolucent control (i.e. not containing any radiopacifier particles). The microcomposite cement was prepared by the addition of 1-µm to 3-µm-size barium sulfate particles (Depuy Orthopaedics) to the basic CMW1 cement powder at 10 weight per cent (wt %), the quantity typically used in standard radioopaque (i.e. radiopacifier particle containing) bone cements. The nanocomposite cement was produced by adding 100-nm-size barium sulfate particles (Sachtleben, Duisburg, Germany) to the basic CMW1 cement powder, also at 10 wt %. Thus, the following cement powder components were prepared: (1) radiolucent CMW1, (2) radiopaque CMW1 microcomposite containing 1-µm to 3-µm-size barium sulfate particles, and (3) radiopaque CMW1 nanocomposite containing 100-nm-size barium sulfate particles.

Several types of specimens for mechanical and morphological characterization (Table 1) were produced with a standard vacuum mixing technique; the powder and liquid components were combined in an Advanced Cement Mixing System (Stryker Orthopaedics, Mahwah, NJ). A vacuum of 70 kPa was applied to reduce the amount of air trapped in the components, which were then mixed for 1 min at a rate of 1 revolution per second to obtain a homogenous paste. The prepared cement paste was then transferred to a cement gun under vacuum, again to avoid the introduction of air bubbles. The cement was introduced into the molds and left to polymerize at room temperature (21°C) for at least 30 min. After molding, all specimens were screened both optically and radiographically. Specimens containing large flaws such as air bubbles were discarded prior to testing.

Mechanical testing

Uniaxial compression. We used an Instron 4201 servo-hydraulic testing machine to perform ASTM F451-99 (ASTM 1999) standard compression tests on all cement groups to determine Young's modulus of elasticity and yield stress. Testing was performed at a crosshead speed of 24.5 mm/min using a 5-kN load cell. At least 10 samples were tested for each cement composition.

Uniaxial tensile tests. We used an Instron 4201 machine to perform ASTM D638-97 (ASTM 1997) standard tensile tests to determine ultimate stress, strain-to-failure, and work-of-fracture (WOF) (defined by the area under the stress-strain curve). Testing was performed at a crosshead speed of 1 mm/min using a 5-kN load cell. At least 6 samples were tested for each cement composition.

Compact tension tests. We used an Instron 4201 machine to perform compact tension fracture toughness tests in order to determine work-of-fracture. Compact tension specimens utilized the sample geometry proposed by Muratoglu et al. (1995), and the specimen notches were precracked using fresh razor blades. Testing was performed at a crosshead speed of 50 mm/s using a 5-kN load cell. At least 6 samples were tested for each cement composition.

Fatigue testing. Fatigue tests were performed using an Instron 8511 servo-hydraulic press equipped with a custom-built circulating, temperature-controlled water bath. Flat dogbone-shaped specimens were prepared in compression molds. The samples were stored at 25ºC for 48 h and then

notched on opposite sides at the center of the gauge region using a rotating saw of 0.25 mm thickness, so that the cross section of the region between the notches was 6 mm × 5 mm while the cross section of the specimens in the gauge region that was not notched was 6 mm × 10 mm. Thus, the notches concentrated the stress within a volume of 6 mm × 5 mm × 0.25 mm at the center of the gauge region. Thereafter, the specimens were stored at 25ºC in distilled water. They were then mounted on the Instron machine and maintained at 37ºC using a circulating water bath containing distilled water. Each specimen was subjected to a cyclic tensile stress of between 15 MPa and 0.45 MPa (R ratio of 0.03) at a frequency of 2 Hz until the specimen completely failed (i.e. fractured into two separate pieces). Specimens that failed at the grips were discarded from the statistical analyses. At least 8 specimens from each cement group were tested.

Morphological characterization

Low-voltage scanning electron microscopy (LVSEM). We used a JEOL 6320FV field emission low-voltage high-resolution scanning electron microscope (LVSEM) operating at 1 kV with a working distance of 3 mm to examine each type of radiopacifier particle and freeze-fractured samples. The samples were initially precoated with a 10-nm coating of gold-palladium conducting alloy.

Ultra-small angle X-ray scattering (USAXS). We used USAXS to quantify the dispersion of radiopacifier particles in the microcomposite and nanocomposite cements. Sheets of 0.5 mm thickness were subjected to USAXS using 10 kEV X-rays and a beam cross-sectional area of 2 mm × 0.6 mm. The available range of the scattering vector, $q = (4\pi/\lambda)\sin\theta$, was 0.00016 – 0.1 Å-1, where λ = 1.299 Å was the synchrotron X-ray wavelength used and θ is one-half the scattering angle.

Specifically, USAXS scattering curves were obtained by plotting the scattered intensity (I) vs. (q) as shown in Figure 6, where:

$$q = (4\pi/\lambda)\sin\theta$$

such that q equals one-half of the scattering angle and λ is the wavelength of X-rays (2.38 Å). USAXS revealed a substantial scattering intensity due to the presence of both voids (radiolucent cement) and also due to barium sulfate particles (Figure 6). The region of the scattering curve at $q > 0.008$ [Å^{-1}] was curve-fitted to a Power Law function which is:

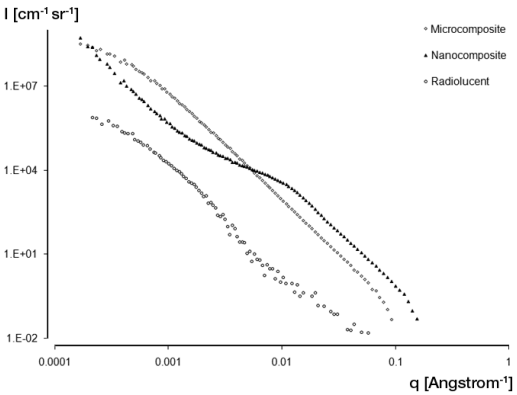

Figure 6. USAXS scattering curves for radiolucent, microcomposite, and nanocomposite cements.

$$I(q) = Kq^{-4}$$

where $K = 2\pi\Delta\rho^2(S/V)$

such that $\Delta\rho$ is the electron density difference between barium sulfate (or voids, in the case of radiolucent cement) and PMMA, and (S/V) is the specific surface area of the scattering entity (radiopacifier or voids). The scattering invariant, Q—defined by the following equation—was calculated for all cement samples using the area under the scattering curve, $q^2I(q)$ versus q:

$$Q = \int_0^\infty q^2 I(q)dq$$

The invariant for an angular range of 0 – qmin was calculated by fitting the low q region of the scattering curve using Guinier's Law and for q_{max} – ∞ using Porod's Law (Glatter and Kratky 1982). The specific surface area (surface area to volume ratio) of dispersed particles within the PMMA matrix can then be defined as: $S/V = \pi(K/Q)$.

A reduction in the specific surface area of radiopacifiers detected by USAXS would imply particle agglomeration. Thus, USAXS can be used to quantify the dispersion of particles within opaque bulk materials such as bone cement in a non-destructive manner. USAXS as a 3-dimensional tool is particularly advantageous in comparison to 2-dimensional imaging methods such as SEM, in that USAXS

Table 2. Material properties, average (SD)

			Radiolucent	Microcomposite	Nanocomposite
Fatigue		Cycles to failure	3188 (1098)	4779 (2227)	9976 (2721)
Compact tension	WOF	N/m^2	564 (138)	566 (106)	476 (100)
Tensile	STF	%	9.1 (1.2)	6.7 (0.95)	9.5 (1.5)
	US	MPa	53 (8.1)	47 (5.1)	52 (5.3)
	Modulus	MPa	681 (93)	554 (226)	655 (153)
	WOF	N/m^2	2.8 (0.7)	1.7 (0.5)	2.9 (0.7)
Compression	YS	MPa	122 (3.6)	124 (1.7)	119 (2.8)
	Modulus	MPa	2202 (299)	2345 (165)	2407 (29)

WOF: work-of-fracture; STF: strain-to-failure; US: ultimate stress; YS: yield stress.

detects the average specific surface area of particles over a relatively large sampling volume of approximately 1 mm^3. In order to reach a comparable sampling volume, several thousand SEM images would have to be obtained and averaged.

Statistics

All groups were first tested for significance with single factor analysis of variance (ANOVA). If significant differences existed among groups, a post-hoc Tukey test was used to detect significant pairwise differences between groups, with the significance level set at 0.05.

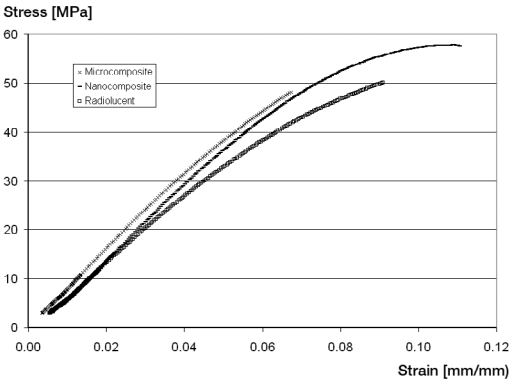

Figure 1. Representative tensile stress-strain plot for bone cement samples.

Results

Static mechanical tests

With compressive testing, no significant differences were detected between the 3 cement groups for elastic modulus (ANOVA, p = 0.08) (Table 2). Also, there were no significant differences in yield stress between the radiolucent and microcomposite groups (t-test, p = 0.2). Yield stress was 4% higher in the microcomposite group than in the nanocomposite group (p = 0.003). All groups exceeded the minimum yield stress required by ASTM F451 (ASTM 1999).

Tensile tests revealed no significant differences between the 3 groups for ultimate stress and elastic modulus (ANOVA, p = 0.3 and 0.4, respectively) (Table 2). Also, there were no significant differences between the radiolucent and nanocomposite groups for strain-to-failure (STF) and work-of-fracture (WOF) (post-hoc test, p = 0.7 and 0.7). Substitution of nanoparticles for microparticles resulted in a 41% increase in STF (p = 0.002), and a 70% increase in WOF (p = 0.005). A plot of the tensile stress/strain curves also revealed characteristics of strain hardening behavior usually seen in more ductile materials. In the nanocomposite group, the curve flattens prior to failure, while the microcomposite graph is typical for brittle failure (Figure 1).

Compact tension testing did not reveal any statistically significant differences in compact tension work-of-fracture between the 3 groups.

Fatigue testing

Fatigue testing showed highly significant differences between the groups tested (ANOVA, p < 0.001). There was no significant difference in fatigue life between radiolucent and microcom-

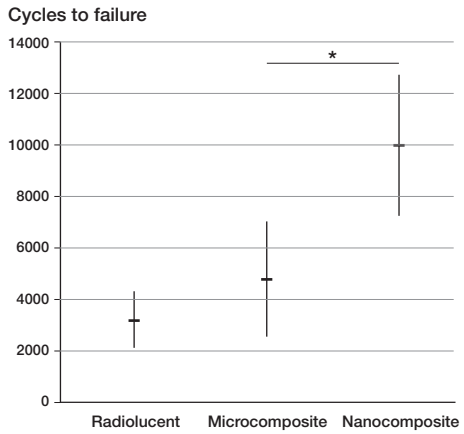

Figure 2. Fatigue life of radiolucent, microcomposite, and nanocomposite cements (cycles to failure, average (SD)).

posite cements (post-hoc test, p = 0.2). The use of nanoparticles increased fatigue life by a factor of 3 when compared to the radiolucent group (post-hoc test, $p < 0.001$), and by a factor of 2 compared to the microcomposite group (post-hoc test, p = 0.001) (Figure 2).

Low-voltage scanning electron microscopy (LVSEM)

LVSEM examination of microcomposite specimens revealed the presence of 0.5-µm to 3.0-µm-size barium sulfate particles, as well as larger particle agglomerates (Figure 3). In nanocomposite samples, LVSEM revealed uniform particle dispersion without agglomerates (Figure 4). There was a higher concentration of features associated with fracture (such as fracture lines) in the nanocomposite cement (Figure 5). These were confined to the inter-bead region containing the nanoparticles, and were not observed in the regions of the prepolymerized beads.

Comparison of LVSEM imaging of fatigue specimen surfaces with those of compact tension specimen surfaces demonstrated that the slower crack propagation during fatigue testing mainly occurred in the inter-bead matrix region. Failure in the rapid-load compact tension tests, however, also occurred through the prepolymerized PMMA beads in the path of the rapidly propagating crack.

Ultra-small angle X-ray scattering (USAXS)

Porod analysis showed that the ratio between the

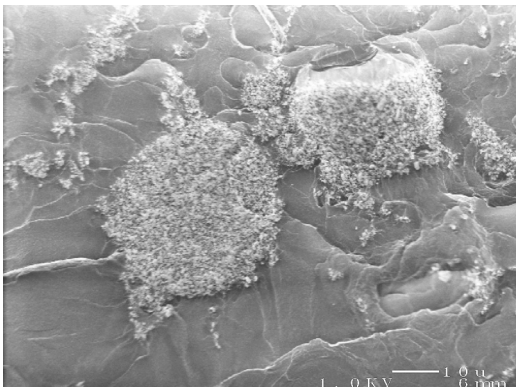

Figure 3. Low-voltage scanning electron micrograph depicting particle agglomerate in microcomposite cement (scale bar represents 10 µm).

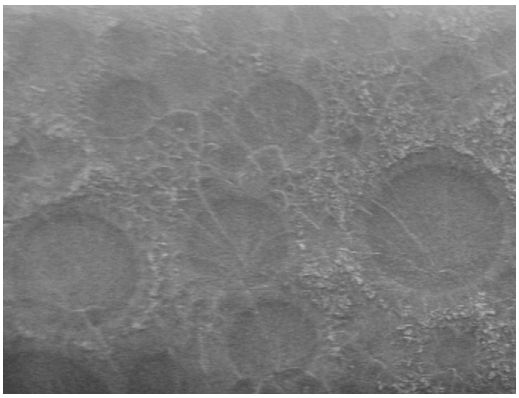

Figure 4. Low-voltage scanning electron micrographs of the fracture surface of a nanocomposite cement specimen (scale bar represents 1 µm).

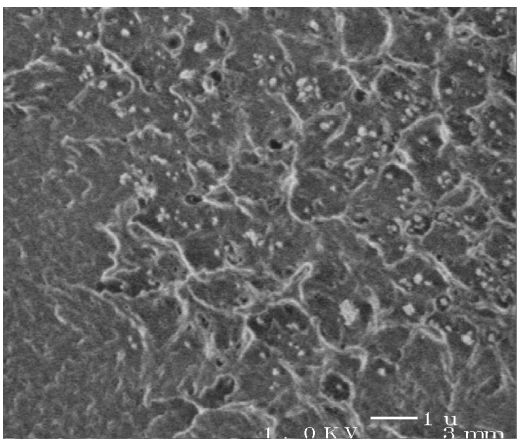

Figure 5. High-resolution low-voltage scanning electron micrograph of the fracture surface of a nanocomposite cement specimen (magnification 10,000×; scale bar represents 1 µm).

Table 3. USAXS specific Surface Areas for PMMA bone cements

Sample	Specific surface area [cm^{-1}]
Radiolucent	6.16147×10^5
Microcomposite	2.39404×10^5
Nanocomposite	2.19348×10^6

specific surface areas of the nanocomposite and microcomposite cements was 9.16 (Table 3).

Discussion

We found that the presence of barium sulfate particles, and the size of these particles, strongly affected the mechanical properties of acrylic bone cement. We observed a 38% reduction in tensile work-of-fracture when micrometer-size barium sulfate particles were added to radiolucent cement, which is in agreement with the results of a previous study that reported a 40% reduction in fracture toughness (Beaumont et al. 1977). The use of uniformly dispersed nanoparticles not only prevented this reduction, but led to a twofold increase in fatigue life.

We conducted long-term cyclic load crack propagation (fatigue) tests, and rapid crack propagation (compact tension) tests to investigate different mechanisms of failure. Nanoparticle substitution had a large effect on fatigue strength, but did not significantly affect compact tension work-of-fracture. LVSEM imaging showed fatigue crack propagation through the inter-bead matrix region of the cement, which lies between the prepolymerized PMMA beads, forms through polymerization of the monomer fluid, and contains the radiopacifier particles. The PMMA in this region is of lower molecular weight than the beads, and therefore less strong mechanically. Reinforcement of this region with nanoparticles resulted in a twofold increase in fatigue strength, possibly due to crack-tip blunting. When the propagating crack encounters a solid particle it is deflected, or stopped, by the particle—a process that dissipates energy. LVSEM demonstrated a larger number of fracture lines in the nanocomposite cement, suggesting that there was extensive crack-tip blunting, probably due to the large number of nanoparticles encountered by the propagating crack. In contrast, the differences in compact tension between the microcomposite and nanocomposite cements were small. Due to the rapid nature of the crack propagation, the cracks propagate through the PMMA beads. Since the beads usually comprise two-thirds of the overall volume of cement and are not particle-reinforced, the influence of the nanoparticles on the overall work-of-fracture decreases.

We also found that USAXS is effective in assessment of particle dispersion within PMMA bone cement by quantitatively measuring the specific surface area of barium sulfate radiopacifiers. The USAXS result of a 9.16-fold increase in specific surface area showed that both microcomposite and nanocomposite cement had relatively well-dispersed radiopacifier particles. LVSEM confirmed the quantitative analysis provided by USAXS measurements, by revealing fracture surfaces where particles were uniformly dispersed throughout the PMMA matrix. The most interesting observation was on the fracture surfaces of the 100-nm size barium sulfate-containing cement. The inter-bead matrix region containing the barium sulfate nanoparticles showed a very high concentration of fracture "craters" approximately 1–2 μm in diameter with a rim made up of "tufts" of plastically deformed PMMA. This indicates that the PMMA surrounding the particles was subjected to plastic strain prior to crack propagation. This is in agreement with the results of our tensile tests, which showed a higher WOF in the nanocomposite cement. Thus, the dispersed barium sulfate nanoparticles set up the PMMA matrix to plastically deform (although only to a small extent) during crack propagation, thereby exhibiting a "nanotoughening" effect. While these differences in WOF and the amount of plastic deformation are not large compared to rubber-toughened PMMA, they have broad implications for fatigue crack propagation rates, which is a concern for the application of bone cements in cemented joint replacement prostheses.

One possible limitation of our study is the use of CMW1 bone cement. This cement is based on pure PMMA, whereas other cements such as Simplex P bone cement (Stryker Orthopaedics) utilize PMMA copolymers, which are known to show better fatigue strength. It is also more viscous than

other cements, which has been attributed to worse handling and mixing characteristics such as the introduction of air bubbles. CMW1 was the only commercial bone cement available without a premixed radiopacifier, thus enabling us to substitute nanoparticles for the conventional, larger particles used. Our results have demonstrated the importance of reinforcing the inter-bead matrix, which is very similar in current bone cements and typically contains lower molecular weight PMMA than the powder particles—and is consequently less tough. Since the nanoparticles are only present in—and therefore exclusively strengthen—the inter-bead matrix, it is to be expected that even copolymer cements could be further improved with this technique. Furthermore, we used radiographs in order to discard samples with large bubbles, to ensure that the results would reflect the properties of the material rather than impurities. This situation is unlike the clinical application, where the introduction of air bubbles is common during cementing of the femoral canal. Sample screening, however, is routine in materials research and we believe that in clinical practice, a strengthened cement matrix will be more forgiving of inadvertently introduced impurities such as air bubbles or biological material. Lastly, fatigue samples were tested in water according to published guidelines. It might, however, be preferable to perform testing in serum to simulate the in vivo environment more closely.

In conclusion, the use of barium sulfate radiopacifier nanoparticles led to a twofold increase in the fatigue life of a commercial acrylic bone cement. This could lead to improved cement performance and implant longevity, while retaining the known and thoroughly characterized chemical structure of current bone cements. However, these cements must be more rigorously fatigue tested under conditions that simulate their in vivo loading and biological environments before being implemented in clinical practice.

Contributions of authors

AHG, WF, and AB were principal investigators involved in the study design, data collection and analysis, and manuscript preparation. RDS and TST were associate investigators involved in the study design, and provided consulting advice during data collection, interpretation of the data, and manuscript preparation.

Acknowledgement

This study was funded in part by the Orthopaedic Research and Education Foundation (OREF), and the Association of Bone and Joint Surgeons (ABJS) through a Marshall R. Urist resident research grant; additional support was provided by the Brigham Orthopaedic Foundation. We thank Dr David Baker and Professor Lisa Pruitt (Dept. of Mechanical Engineering, University of California at Berkeley, Berkeley, CA) for their assistance and expertise in fatigue testing, and Peter Jemian and Jan Ilavsky (UNICAT) for their assistance with USAXS measurements. The UNICAT facility at the Advanced Photon Source (APS), Argonne National Laboratory, Argonne, IL, is supported by the Materials Research Laboratory, University of Illinois at Urbana-Champaign, (US Department of Energy, the State of Illinois-IBHE-HECA, and the National Science Foundation), the Oak Ridge National Laboratory (US Department of Energy), the National Institute of Standards and Technology (US Department of Commerce), and UOP LLC. The APS is supported by the US Department of Energy, Office of Science, Office of Basic Energy Sciences, under contract no. W-31-109-ENG-38.

No competing interests declared.

ASTM 1997. D638-97 Standard Test Method for Tensile Properties of Plastics.

ASTM 1999. F451-99 Standard Specification For Acrylic Bone Cement.

Beaumont P W R, Jolliffe V, Gore D. Fracture of particulate composites based on polymethylmethacrylate. Fracture 1977; 3: 1015-23.

Demian H, McDermott K. Regulatory perspective on characterization and testing of orthopedic bone cement. Biomaterials 1998; 19: 1607-18.

Glatter O, Kratky O. Small angle X-ray scattering. Academic Press New York 1982.

Krause W, Mathis R S. Fatigue properties of acrylic bone cement: a review of the literature. J Biomed Mater Res. Appl Biomat 1988; 22 (A1): 37-53.

Lewis G. Fatigue testing and performance of acrylic bone-cement materials: state-of-the-art review. Biomed Mater Res. Part B. Appl Biomat 2003; 66 (1): 457-86.

Muratoglu O K, Argon A S, Cohen R E, Weinberg M. Microstructural fracture processes accompanying growing cracks in tough rubber-modified polyamides. Polymer 1995; 36 (25): 4787-95.

Saha S, Pal S. Mechanical properties of bone cement: a review. J Biomed Mater Res 1984; 18 (4): 435-62.

Topoleski L D, Ducheyne P, Cuckler J M. A fractographic analysis of in vivo poly(methyl methacrylate) bone cement failure mechanisms. J Biomed Mater Res 1990; 24 (2): 135-54.

Topoleski L D, Ducheyne P, Cuckler J M. Microstructural pathway of fracture in poly(methyl methacrylate) bone cement. Biomaterials 1993; 14 (15): 1165-72.